International Journal of Heat and Mass Transfer 66 (2013) 261–270

Contents lists available at ScienceDirect

International Journal of Heat and Mass Transfer

journal homepage: www.elsevier.com/locate/ijhmt

Characterization of pool boiling mechanisms over micro-patterned surfaces using PIV

E. Teodori, A.S. Moita *, A.L.N. Moreira

Instituto Superior Técnico, Department of Mechanical Engineering, Lisbon, Portugal

ARTICLE INFO

Article history:
Received 25 October 2012
Received in revised form 10 July 2013
Accepted 10 July 2013
Available online 3 August 2013

Keywords:
Pool boiling
Heat transfer
Bubble dynamics
PIV
Interaction mechanisms
Micro-patterned surfaces

ABSTRACT

The present work addresses hydrodynamic and heat transfer processes of pool boiling over surfaces patterned with micro-cavities, in the context of cooling applications. The cavities are square and have a fixed depth. The variable considered here is the distance between cavities 200 μm < S < 2000 μm. The results show that to assure an effective improvement of the heat transfer, the design of the micro-patterns must balance the positive effect of the micro-patterns in promoting the activation of the nucleation sites with the negative effect of an excessive interaction between them. Particular emphasis is given to the horizontal coalescence of the departed bubbles close to the wall, which is observed to cause the deterioration of the heat transfer coefficient, due to the formation of large vapor bubbles that isolate the surface from the liquid.

An innovative analysis of the boiling process from micro-patterned surfaces is proposed here, which combines image post-processing with PIV measurements. Evaluation of the characteristic bubbles velocity obtained by PIV measurements evidences that the optimal pattern which balances the positive effect of increasing the parcel of liquid evaporation and the negative effect of the horizontal coalescence (with a distance between cavities S = 400 μm) also allows a more stable vertical bubble velocity, thus removing the vapor from the surface. However, the velocity of the bubbles for these surfaces is quite low, when compared to that of surfaces with a smaller number of cavities, i.e. with larger S. Hence, the convection induced by bubble motion is reduced in these optimal patterned surfaces, although the heat transfer coefficient is the highest. In line with this, one may argue that the positive effect of increasing nucleation sites (under controlled coalescence) considerably improves the latent heat parcel, which is dominant. This may be so, since the surface pattern promoting the largest velocities (C7, S = 1200 μm) has the lowest heat transfer coefficient, given the lowest number of active nucleation sites. Additionally, destabilization of the bubbles velocity is induced in this surface, which actually contributes to the deterioration of the heat transfer coefficient.

1. Introduction

Several thermal management strategies have been explored within the last years in the context of the cooling of electronic components. Pool boiling is a very attractive solution, given its effectiveness and its hardware simplicity. Such effectiveness is due to the particular mechanism of heat transfer which involves three parcels, namely the natural convection from the heating surface to the fluid, the bulk convection induced by bubble growing and detachment and the vapor convection directly transferred into the bubble from the surface [1]. The relative importance of these parcels depends on the thermo physical properties of the working fluids, on the geometry of the system and on bubble dynamics, which affects the convective flow and naturally, the parcel of latent heat. One of the most popular strategies to improve pool boiling heat transfer is altering surface topography, based on the argument that it increases the liquid–solid contact area, increasing the parcel of convection and promotes the appearance of active nucleation sites within the heterogeneous nucleation process (*e.g.* [2]), thus contributing to increase the parcel of latent heat. While the first is an obvious benefit, the latter is not so straightforward. In fact, a larger number of active nucleation sites should promote the bulk convection induced by bubble detachment and the vapor convection, but it also endorses several interaction mechanisms between nucleation sites, which may enhance or actually inhibit it, so that the negative effects of such interaction can overcome the potential advantages. These interactions are particularly intense at high heat fluxes, which are the main target in the cooling of high energy density systems. Nevertheless, apart from pioneering work of Chekanov [3], Sultan and Judd [4] and more recently Zhang and Shoji

* Corresponding author. Tel.: +351 21 841 78 51; fax: +351 21 841 61 56.
E-mail addresses: e.teodori@dem.ist.utl.pt (E. Teodori), anamoita@dem.ist.utl.pt (A.S. Moita), moreira@dem.ist.utl.pt (A.L.N. Moreira).

0017-9310/$ - see front matter © 2013 Elsevier Ltd. All rights reserved.
http://dx.doi.org/10.1016/j.ijheatmasstransfer.2013.07.033

[5], the interaction mechanisms are still sparsely reported in the literature. The existing studies consider surfaces with 1, 2 and 3 custom made cavities. The relation between the dimensionless cavity spacing S/D – i.e. the ratio of the cavity spacing to the average bubble departure diameter and the average bubble departure frequency f were the parameters used to identify several interaction regions. However, each author identifies different regions. The most unifying theory was proposed by Zhang and Shoji [5] who associated the interaction regions, also as a function of S/D, with the relative importance of three competitive effects, namely the hydrodynamic interaction between bubbles, the thermal interaction between nucleation sites and the horizontal and declining bubble coalescence. The main limitation of these studies is the very restricted number of cavities which turns difficult any extrapolation to the rough surfaces used in practical applications. In this context, the present work stands for the use of numerous micro-cavities (although this number is well established).

Recent studies, based on a limited number of micro-cavities or micro-pillars (*e.g.* [6,7]) allowed to relate the decline of the heat transfer coefficient observed at high heat fluxes (but still far from the Critical Heat Flux conditions) with the formation of large vapor bubbles, induced by the occurrence of horizontal coalescence among nucleation sites. These large bubbles, which isolate the surface from the liquid, also reduce the induced liquid motion. This suggests that especially for higher heat fluxes, an optimal pattern of the structural elements can be obtained, which besides augmenting the liquid/solid contact area, keeps the inhibitive interaction among nucleation sites under acceptable intensity, thus ensuring an overall improved cooling performance. This may be so, since in recent work, Nimkar et al. [8] propose the establishment of an optimum inter-cavity spacing, for which most of the surface remains active for a wide range of heat fluxes, although the authors are not very clear on the arguments sustaining this optimum spacing.

In line with this, the work presented here addresses a detailed study of boiling on surfaces micro-patterned with artificially created cavities, to quantify the effect of the surface topography on the interaction mechanisms, and particularly on the horizontal coalescence. Special emphasis is given to understand how the interaction mechanisms affect bubbles dynamics and consequently the various parcels of the pool boiling heat transfer, as identified by Han and Griffith [1]. Describing the flow induced by the bubbles motion is vital, since Han and Griffith [1], one of the few studies analyzing the relative importance of the various heat transfer parcels, report that the convection induced by bubble motion may represent a relative importance of nearly 80%, comparing to the latent heat and to the natural convection parcels. In the work presented here the analysis of the flow is performed using PIV. Few studies in the literature confirm the potential of using PIV to measure bubble velocity inside a flowing fluid, as for example reported by Sasaki et al. [9] and Cheng et al. [10], although they focused mostly on the characterization of the plume, far away from the surface. In the present work, bubble detachment and induced convection velocities are investigated using PIV, at different distances from the surface. Besides the highly non uniform characteristics of boiling flows which turn them difficult to describe (particularly with PIV, which is very sensitive to them), one major challenge to overcome was to establish the measurement planes which are close enough from the surface, to provide information to be related to the bubbles detachment, while assuring the required measurement accuracy.

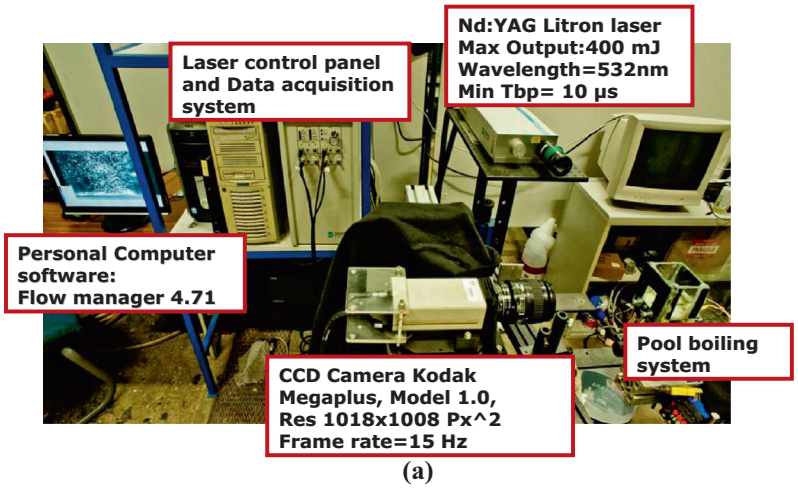

Fig. 1. Experimental set-up. (a) Global view. (b) Detail of the pool boiling section. (c) Zoom picture taken inside the pool boiling section. Boiling only occurs over the micro-patterned surface.

2. Experimental approach

2.1. Experimental set-up

The experimental arrangement mainly consists on a power supply, a heating block, a pool boiling test section, a high-speed camera (Phantom v4.2 from Vision Research Inc., with 512 × 512 pixels at 2100 fps and a maximum frame rate of 90 kfps), a temperature acquisition system and a PIV system. For visualization, backlight illumination is provided by a 450 W LED spotlight, passing through a diffusing glass to homogenize the background light. Type-K thermocouples are used to monitor and acquire the temperature and evaluate the heat flux. The signals of the thermocouples are sampled with a National Instruments DAQ board plus a BNC2120 and amplified with a gain of 300 before processing. The acquisition frequency is 100 Hz and the temperature is monitored for 20 s after reaching a stable condition of the system that, in this case, has been represented by a constant temperature variation of ±0.5 °C. The heating module consists on a copper support, insulated by fiberglass and heated by two electric cartridge heaters. The temperature distribution of the copper support has been evaluated by means of temperature measurements with a range of imposed heat flux. The heat losses evaluated for this configuration are 37% in the worst case. The micro-patterned surfaces are placed on the top of the copper support. These surfaces, which have an area of 1 cm^2, are made from silicon wafers with a thickness of 380 μm. The amount of liquid is 7 ml. The boiling section, placed over the copper support is made of glass and sealed with rubber and high temperature silicone. It has an area of 7.05 cm^2 and a height of 15 mm. An overview of the entire set-up is depicted in Fig. 1. Detailed description of the experimental set-up is provided in [7,11,12].

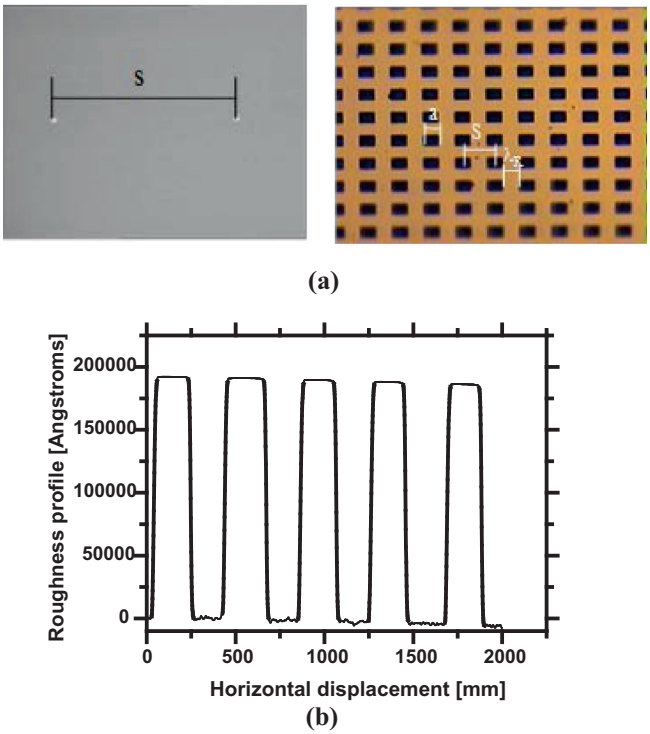

Fig. 2. (a) Detail of a micro-patterned surface, showing the definition of the dimensions a, λ_R and S characterizing its topography. h_R is the depth of the cavities, which can be evaluated from the roughness profile, illustrated in (b).

Table 1
Summary of the main range of the topographical characteristics used in the customized micro-patterned surfaces. N_{cav} is the number of cavities in the entire surface.

Material	Reference	a [μm]	h_R [μm]	S [μm]	λ_R [μm]	N_{cav}
Silicon wafer	Smooth	≈0	≈0	≈0	≈0	≈0
	C1	52	20	464	260	441
	C2	52	20	626	340	256
	C3	52	20	304	177	1089
	C4	52	20	400	452	625
	C5	52	20	700	752	196
	C6	52	20	800	852	144
	C7	52	20	1200	1252	64

2.2. Characterization of the micro-patterned surfaces

The micro-patterns are printed over the silicon wafer by lithography and are custom made, combining wet etching with plasma etching. At this stage of the research, given the high number of variables related to surface patterning that can be altered, one decided to fix the shape, size and depth of the cavities. So, the cavities are squares with side length a = 52 μm. Depth h_R = 20 μm, varies within a range that does not affect the boiling mechanisms. By the current manufacturing procedure, this shape, size and depth can be accurately controlled and one knows from previous experiments [7] that they work as nucleation sites. The distance between the centers of the cavities S, is the variable and ranges between 304 μm < S < 1200 μm. The distance S was chosen for now as the variable parameter since one wishes to further investigate the effect of the interaction mechanisms, observed in [7], particularly the horizontal coalescence and S is recognized in the literature (*e.g.* [4,5]) as being a vital parameter.

These quantities, which are defined in Fig. 2 are measured directly from the roughness profiles, obtained using a mechanical profile meter, with a measurement precision of ±100 Å. The main topographical characteristics of the surfaces used here are summarized in Table 1.

The wettability of the surfaces was also characterized, based on the static contact angle θ, following the approach of many authors (*e.g.* [13]).

The contact angles are measured at room temperatures, inside a thermostatted ambient chamber (Ramé-Hart Inc., USA, model 100-07-00), using the Sessile Drop Method. Images of the deposited droplet are recorded with a JVC Color T-1079 video camera mounted on a Wild M3Z microscope, with a magnification of 40 times. An average value is considered for each pair liquid-surface which is determined from at least five measurements taken at different regions of the surface. The time evolution of the average contact angles is obtained by curve fitting and the final values are determined by extrapolation. The detailed measurement procedure has been described in previous works (*e.g.* [14]).

It is worth noting that this is the apparent wetting angle of liquid droplets deposited over the surfaces and not the local angle defined at the departure of the gas bubbles. The cavities do not al-

Table 2
Thermo-physical properties of the liquids used in the present study, taken at saturation, at 1.013 × 10^5 Pa.

Property	Ethanol	Water
T_{sat} [°C]	78.4	100
ρ_l [kg/m^3]	736.4	957.8
ρ_v [kg/m^3]	1.647	0.5956
μ_l [mN m/s^2]	0.448	0.279
C_{pl} [J/kg K]	3185	4217
k_l [W/mK]	0.165	0.68
h_{fg} [kJ/kg]	849.9	2257
σ_{lv} [N/m] × 10^3	17	58

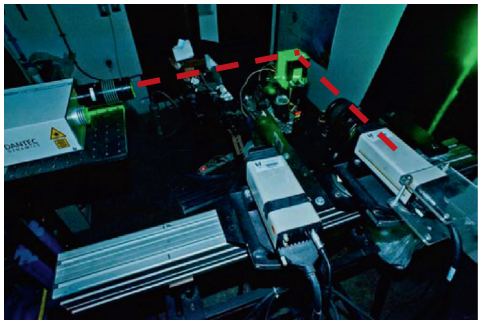

(a)

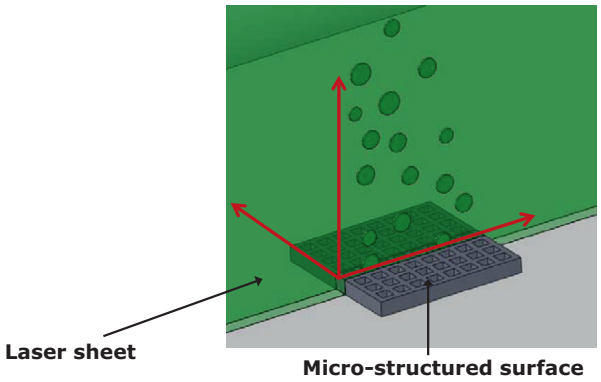

(b)

Fig. 3. (a) PIV arrangement. (b) Coordinate system.

ter significantly the apparent equilibrium contact angle, which is always $\theta \approx 0°$ for all the surfaces wetted with ethanol and varies between $60.5° < \theta < 91.5°$ when the surfaces are wetted with water.

2.3. Methodology and working conditions

Pool boiling is investigated for different liquids, namely ethanol and water, to account for the liquid properties as well as to infer on the additional effects of wettability in the observed phenomena. Table 2 depicts the thermo-physical properties of the liquids used in the present study.

Heat flux and heat transfer coefficients are determined for the various liquid/surface pairs. Afterwards, they are related to the bubble dynamics, which is quantified by the bubble departure diameter and frequency, active nucleation sites density, bubble growth rates and bubble velocities. This characterization is made by combining high-speed visualization with PIV measurements. To quantify the effect of horizontal coalescence, several dimensionless parameters are used, which were introduced in a previous study (*e.g.* [11,12]).

Each boiling curve presented for every liquid and every heating surface used here are averaged from seven experimental curves. The curves are obtained by varying the imposed heat flux in steps of 15 W/cm^2. The temperature measurements are taken for each heat flux step when the system is considered to attain equilibrium, i.e. when the temperature oscillation is ±0.5 °C. Before each experiment, the liquid is degassed by maintaining it in the pool 20 °C above the saturation temperature.

Experiments were conducted to obtain average boiling curves by both increasing and decreasing the heat flux, to infer on hysteresis effects, as pointed for instance by Mohamed and Bostanci [15]. The temperature measurements have an uncertainty of ±1 °C. The relative error associated with the determination of the heat transfer is 5%.

2.3.1. Bubble dynamics – image analysis procedure

Following the approach presented in the most of the works reported in the literature, the bubble nucleation parameters selected in the present study are the bubble departure diameter, the bubble departure frequency and the active nucleation sites density. This characterization is based on high-speed visualization and image post-processing. The images are recorded with a frame rate of 2200 fps. For the optical configuration used here, the spatial resolution is 9.346 μm/pixel.

The bubble departure diameter is measured for each test condition from 300 to 1060 frames. For each image a mean value is averaged from 5 to 16 measurements for every nucleation site that is identified in the frame.

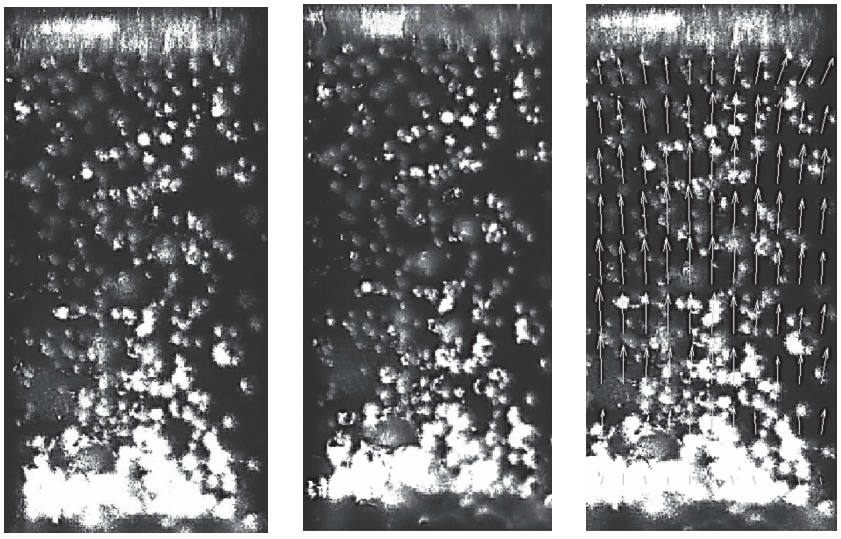

(a) (b) (c)

Fig. 4. Example of image analysis by average cross correlation: (a) frame corresponding to the first laser pulse, (b) frame corresponding to the second laser pulse, and (c) flow field obtained after applying average correlation algorithm.

At higher heat fluxes, the various interaction mechanisms, which will be discussed in the following section, may alter significantly the value of the departure diameter, especially when horizontal coalescence occurs. Therefore, in those cases, the measured diameters are a mean value taken from the averaged diameters, which are evaluated after the occurrence of such events close to the wall.

The error associated to the measurements of the bubble departure diameter is ±9.346 μm.

The bubble departure frequency is estimated by determining the time elapsed between apparent departure events, which are counted for a defined interval of time. The departure frequency is assessed, for each test condition, for at least five nucleation sites, which are evaluated based on extensive image post-processing of 300 to 1060 frames. The final value of the bubble departure frequency is the average between the frequencies of each nucleation site. The uncertainty associated to these measurements is ±1 fps.

Finally, the evaluation of the active nucleation sites density must be done by visual inspection of the frames, which introduces an uncertainty associated to the subjective criterion of the observer. To lessen this uncertainty, at least ten frames are chosen, at different times during the single experiment. The final values of the active nucleation site density are an average of the ten evaluated values.

2.3.2. PIV measurements

Several studies in the literature confirm the potential of using PIV to measure bubble velocity inside a flowing fluid, as for example reported by Sasaki et al. [9] and Cheng et al. [10]. However, the results obtained from this technique are very sensitive to the characteristics of the flow and to the parameters used during the visualization and the post-processing of the images (*e.g.* [10]). In the present work, the main focus is to measure the velocity of the bubbles, so seeding was not used, but instead the bubbles are followed, as suggested by Cheng et al. [10]. The bubble diameter of ethanol is in the range of 500–800 μm, measured by image post-processing. These dimensions and the low characteristic velocities of the bubbles (1–10 cm/s) require a careful analysis of all the parameters which have to be selected in the PIV configuration. The PIV system uses a CCD camera Kodak Megaplus, Model 1.0, with an image resolution of 1018×1008 pixel^2. The bubbles are illuminated via a dual Nd:YAG Litron laser. The PIV arrangement and the coordinate system considered in the measurements are shown in Fig. 3.

The time delay between laser pulses is varied ($1 < \Delta t < 8$ ms) depending on the imposed heat flux: the time between pulses is smaller for higher imposed heat fluxes. Furthermore, the interrogation area and the overlap are also varied for the various imposed heat flux conditions, in an optimization process, to assure that the chosen values are adequate to obtain accurate measurements. Hence, the selected interrogation area was varied between 16 and 64 pixels (1 pixel/58 μm) to assure that at least five bubbles are inside. An overlap of 50% is chosen by analyzing two consecutive frames and evaluating the average displacement of the bubbles. The most appropriate approach for this kind of flow is using a recursive cross correlation or the average correlation algorithms (*e.g.* [10]). In the present work, after analyzing extensively both approaches, the cross correlation was considered to be the most appropriate. Fig. 4 represents a typical flow field obtained. The measurements performed using PIV are compared with extensive image post-processing, within quite good agreement. The PIV data were processed with the software Flow manager 4.2.

3. Results and discussion

The present study is part of a work aimed at optimizing pool boiling heat transfer for cooling applications, using micro-patterned surfaces. The micro-patterns must be designed to optimize the heat transfer by balancing the positive aspect of the micro-cavities in increasing the number of active nucleation sites and the negative effect that horizontal coalescence introduce both in the deterioration of the heat transfer due to the increase of vapor cushion near the wall and in the possible modifications it can introduce in the convective flow induced by the bubbles (*e.g.* [12]). In line with this, a short summary of the quantification of the effect of the horizontal coalescence in several parameters such as the departure frequency and the convection heat transfer is introduced in the first sub-section. Then the main focus of the results presented in the subsequent sub-paragraph is in the characterization

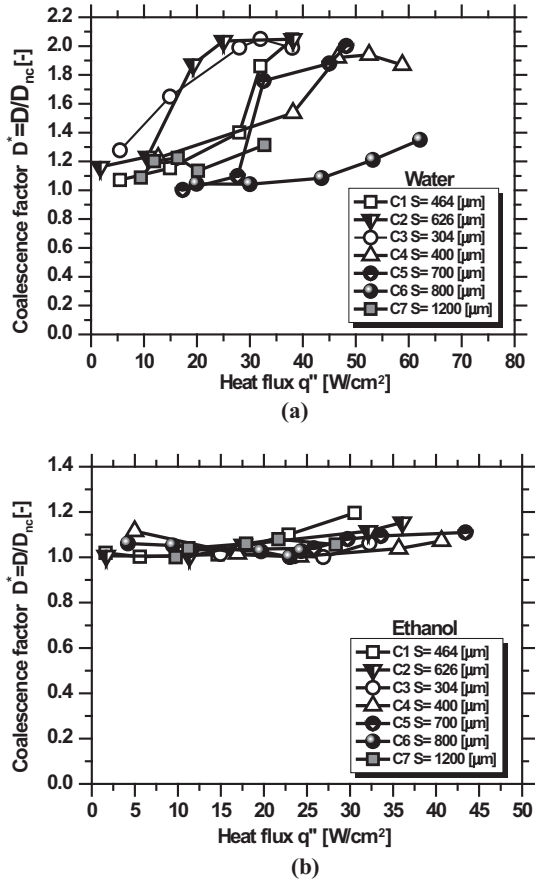

Fig. 5. Coalescence factor versus heat flux for: (a) water, (b) ethanol.

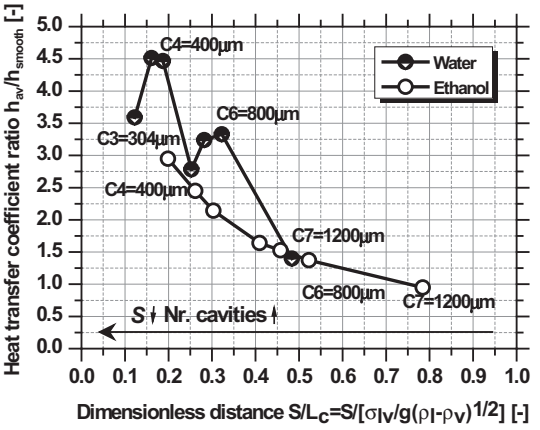

Fig. 6. Heat transfer ratio versus dimensionless distance for water and ethanol in the range of the patterns studied.

Table 3
Complete panoramic of all the characteristics and main PIV parameters for the smooth surface t_{bp} is the time between pulses and I.A is the interrogation area.

No.	Heat flux [W/cm^2]	Heat transfer coefficient [W/cm^2 K]	Bubble departure diameter D [mm]	Characteristic velocity $V_{H/D=10-20}$ [cm/s]	t_{bp} [ms]	Corr. type	I.A [Px]	Overlap %
1	35.91	1.186582	1.26	8.9	3	Cross	64	50
2	30.16	1.139484	1.19	7.47	3	Cross	64	50
3	29.66	1.192216	1.21	5.86	3	Cross	64	50
4	18.09	1.205537	0.99	4.65	5	Cross	64	50
5	20.89	1.187963	1.19	3.9	3	Cross	64	50
6	10.54	0.955608	0.78	2.52	5	Cross	64	50
7	8.11	1.053937	0.74	2.02	8	Cross	64	50
8	1.79	0.84079	0.72	1.44	8	Cross	64	50

of the flow, namely on the average vertical bubble velocity, determined from PIV measurements. Finally, the third sub-paragraph relates the bubble dynamics with the bubble velocities to understand how they affect the parcels composing pool boiling heat transfer and sub-subsequently, the convective heat transfer coefficient, for the various micro-patterns.

3.1. Effects of horizontal coalescence

Bubble dynamics was described using high-speed visualization and image post-processing to quantify characteristic quantities such as the bubble departure diameter, the departure frequency and the active nucleation sites density. There is a clear deterioration of the heat transfer coefficient caused by overstated horizontal coalescence (*e.g.* [7]). In this context, the coalescence factor $D^* = D/D_{nc}$ was introduced by the authors to quantify the intensity of horizontal coalescence in the boiling of different liquids over various micro-patterned surfaces. The results are depicted in Fig. 5.

As described in detail in [11,12], the coalescence factor, defined by the ratio between the average bubble departure diameter (including coalescence) and the single diameter of the bubbles which exit the cavity with no coalescence is usually larger than 1 for liquids with large surface tension, such as water and very close to 1 for liquids with smaller surface tension. Hence, stronger coalescence occurs during water boiling in opposition to ethanol. Additionally, the distance between the cavities S can promote coalescence. Against intuition, the coalescence factor does not increase as S decreases. Instead, there is an optimum range, which naturally, is a function of the liquid surface tension (*e.g.* [11]). Further introducing the departure frequency as a variable, it is clear that there is a maximum value of f, which can be related to an optimum distance S, which keeps the coalescence under controlled activity. Finally, the active nucleation sites density must also be considered as it introduces the relative importance of the latent parcel of heat removed during vaporization. An extensive analysis of these parameters is out of the scope of the present paper, but can be found in [11,12]. Such analysis suggests that there is an optimum spacing S to balance the occurrence of coalescence with the promotion of active nucleation sites. This trend can be identified on the map depicted in Fig. 6. This map represents the heat transfer performance of a micro-patterned surface, referenced to the smooth one, as the ratio between the average heat transfer coefficients h_{av}/h_{smooth}, as a function of the distance S, made dimensionless with the characteristic length scale L_c, from Fritz's equation [16], that already includes the effect of the various properties swiftly discussed above. $L_c = (\sigma_{lv}/g(\rho_l - \rho_v))^{1/2}$, where g is the gravitational constant and ρ_l and ρ_v are the liquid and vapor specific masses, respectively.

One may interpret the curves in Fig. 6 with the help of Fig. 5, as follows: for the fluid with the highest surface tension, in which the coalescence effects are stronger, looking at the evolution of the curve in Fig. 6, from the largest to the smallest values of S/L_c, the distance between cavities S decreases and consequently the number of cavities increases. Hence, using the surface with the largest S (C7, $S = 1200$ μm), does not promote horizontal coalescence, as shown in Fig. 5(a), but renders a very small improvement of the heat transfer (h_{av}/h_{smooth} is just slightly above 1). The contribution of the micro-cavities to promote boiling and consequently increase the latent heat parcel removed by liquid evaporation is very low. As S decreases, the horizontal coalescence becomes more intense (Fig. 5(a)), but the positive effect of the increasing number of micro-cavities in promoting boiling is still dominant, so h_{av}/h_{smooth} increases in Fig. 6, for lower values of S/L_c. An absolute peak can be identified at $0.31 < S/L_c < 0.37$ (corresponding to the micro-patterned surface C4, with $S = 400$ μm). This peak establishes the limiting pattern with the optimum distance between the micro-cavities, which balances the positive effect of increasing the parcel of liquid evaporation and the negative effect of the horizontal coalescence. Further decreasing S the effect of the coalescence becomes dominant and quickly gives rise to very large vapor bubbles, which isolate the surface from the liquid. As a consequence, further decreasing S bellow this optimum range renders in the considerable decrease of h_{av}/h_{smooth}.

A similar trend is observed for the fluid with the smallest surface tension (ethanol), but in this case, as the horizontal coalescence is much less intense (Fig. 5(b)), the maximum is expected to be reached at a lower value of S/L_c, which was not achieved with the surfaces used in the present study.

The discussion promoted from Figs. 5 and 6 mainly relates the micro-patterning of the surfaces with the parcel of the heat transferred at bubble growth and liquid vaporization. However, the micro-patterns also affect the bubbles' velocity thus influencing the parcel of the induced convection. To infer on this effect, one must characterize the flow, as discussed in the next subsection.

3.2. Flow description: analysis of the average vertical bubble velocity

The effect of the surface patterning in the parcel of the induced convection was investigated evaluating the average vertical bubble velocity (average of the velocity profile for a fixed value of H/D), along the vertical dimensionless distance H/D, where H is the vertical distance from the top face of the surface in (mm) and D is the bubble departure diameter (also in mm), for different heating conditions and different micro-patterns. Naturally that this effect is relevant close to the surface, but given the well known restrictions of PIV measurements performed very close to the surface (*e.g.* [17]) the assessment of bubbles' velocity must be performed at various distances H/D, in order to understand bubbleś motion. Here, one will start from the smooth surface and then will progressively increase the number of cavities (i.e. decreasing S), following the trend discussed during the analysis of Figs. 5 and 6. Based on that discussion, three representative micro-patterns were selected: the one with the largest distance between cavities ($S = 1200$ μm), one with intermediate distance ($S = 800$ μm), and the best performing

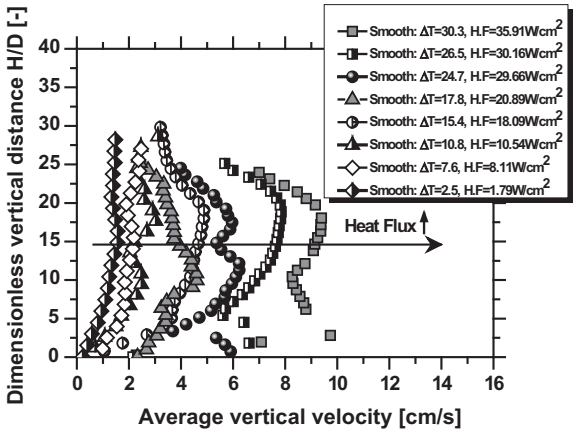

Fig. 7. Average vertical velocity versus dimensionless vertical distance for the pool boiling of ethanol on the smooth surface. Here, $\Delta T = T_w - T_{sat}$ and H.F. is the imposed heat flux.

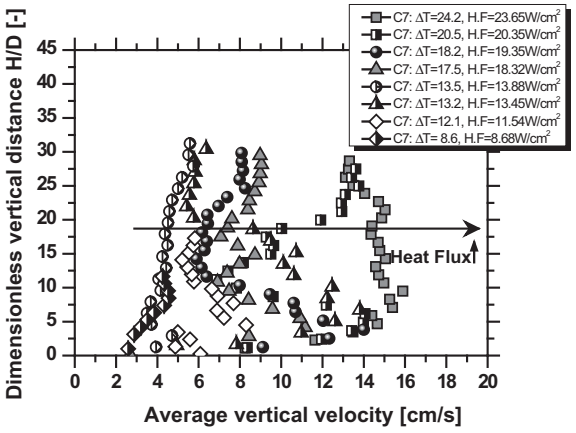

Fig. 8. Average vertical velocity versus dimensionless vertical distance for ethanol on the surface C7 ($S = 1200$ μm). $\Delta T = T_w - T_{sat}$ and H.F is the imposed heat flux.

micro-pattern, identified by the maximum for water in Fig. 6 ($S = 400$ μm), which is also one of the best performing surfaces for ethanol.

Hence, starting with the smooth surface, which is taken as a reference, Table 3 depicts the detailed characterization of the measurements made. From the left side, first columns show the heat transfer parameters (heat flux and heat transfer coefficient). The characteristic velocity obtained with PIV measurements (i.e. the value of the velocity in the vertical position where the bubble reaches the constant velocity) is presented in the 4th column. Finally, some of the relevant parameters set for the PIV configuration are shown, namely the time between laser pulses t_{bp}, the correlation type, the side of the interrogation area I.A and the overlap used.

Fig. 7 depicts the average vertical velocity of the bubble versus the dimensionless distance H/D, for different heating conditions, for the pool boiling of ethanol on the smooth surface. Starting from $H/D \approx 0$ (top face of the heating surface), the bubble velocity increases until reaching an almost constant value which remains stable for increasing values of H/D. A slight increase of the vertical velocity occurs for $10 < H/D < 18$ as one increases the imposed heat flux and then decelerates due to the braking effect forced by the zero velocity at the top of the pool. As the imposed heat flux is higher, the bubbles are ejected with larger average velocity but then quickly slow down, since the plume becomes wider so this breaking effect starts to occur at lower values of H/D. Due to the small number of nucleation sites on the smooth surface, the interaction among them is negligible, so the vertical velocity is not much disturbed. This explains the constant value observed for the wide range of H/D.

The first micro-patterned surface to be analyzed is the one with the largest distance among cavities, thus with the smallest number of cavities (surface C7, $S = 1200$ μm). Table 4 summarizes the relevant parameters for the analysis of the results. Here, 4th and 5th columns add the bubble departure frequency and the product $f \cdot D$, which could not be accurately determined for the smooth surface, given the very small number of active nucleation sites. $f \cdot D$ provides a sort of reference value for the velocity, which is actually quite close to those obtained from the PIV measurements, particularly for lower imposed heat fluxes.

The average vertical bubble velocity versus the dimensionless distance H/D obtained for the pool boiling of ethanol on surface C7 ($S = 1200$ μm) is depicted in Fig. 8, for various imposed heat fluxes.

The presence of preferential nucleation sites on the surface increases the complexity of the phenomena involved and thus of the analysis. Generally, one may observe that the velocity increases with the heat flux. The evolution of the vertical velocity with H/D follows a complex trend: it starts to increase from $H/D = 0$ up to $H/D = 10$ and then assumes a constant value, as for the smooth surface. However, in this case, strong oscillations of the velocity occur around an average value, which starts very close to the wall and keeps clearly identified between $10 < H/D < 20$. The magnitude of these oscillations increases with the heat flux. The number of cavities is sufficient to promote nucleation and there is a week interaction between nucleation sites. Even though the horizontal coalescence is not much strong, the size of the bubbles is high enough to decrease the departure frequency [12]. This effect allied to the interaction between raising bubbles turns the boiling process much more chaotic, when compared to the smooth surface. Consequently, bubbles motion is much more random so that these oscillations will not allow a stable bulk convective flow.

Further decreasing the distance between cavities to $S = 800$ μm (surface C6), one may notice that the order of magnitude of the reference velocity $f \cdot D$ and the characteristic velocity is really similar.

Once again, the most relevant parameters for the analysis are summarized in Table 5.

Table 4
Complete panoramic of all the characteristics and main PIV parameters for surface C7 ($S = 1200$ μm). t_{bp} is the time between pulses and I.A is the interrogation area.

No.	Heat flux [W/cm^2]	Heat transfer coefficient [W/cm^2 K]	Bubble departure diameter D [mm]	Bubble departure frequency f [Hz]	$f \cdot D$ [cm/s]	Characteristic velocity $V_{H/D=10-20}$ [cm/s]	t_{bp} [ms]	Corr. type	I.A [Px]	Overlap %
1	23.65	0.96	0.89	80	7.12	14.71	5	Average	64	50
2	20.35	1.01	0.85	81	6.88	11.45	2	Cross	64	50
3	18.35	1.02	0.8	90	7.20	8.3	2	Cross	64	50
4	19.35	1.01	0.82	89	7.29	6.83	2	Cross	64	50
5	13.45	0.95	0.63	83	5.22	7.65	2	Cross	64	50
6	11.54	0.91	0.57	82	4.67	6.59	3	Cross	64	50
7	13.88	0.98	0.64	83	5.31	4.4	3	Cross	64	50
8	8.68	0.98	0.39	79	3.08	3.99	3	Cross	64	50

Table 5
Complete panoramic of all the characteristics and main PIV parameters for surface C6 (S = 800 μm). t_{bp} is the time between pulses and I.A is the interrogation area.

No.	Heat flux [W/cm^2]	Heat transfer coefficient [W/cm^2 K]	Bubble departure diameter D [mm]	Bubble departure frequency f_d [Hz]	$f \cdot D$ [cm/s]	Characteristic velocity $V_{H/D=10-20}$ [cm/s]	t_{bp} [ms]	Corr. type	I.A [Px]	Overlap %
1	24.72	1.50	0.82	74	6.06	12.82	1	Cross	64	50
2	18.48	1.35	0.81	73	5.91	10.61	1	Cross	64	50
3	36.03	1.60	0.84	77	6.46	8.81	1	Cross	64	50
4	39.70	1.59	0.84	75	6.31	6.15	2	Cross	64	50
5	28.23	1.38	0.84	76	6.38	5.53	1	Cross	64	50
6	5.56	1.24	0.75	65	4.87	3.3	1	Cross	64	50
7	4.91	1.04	0.74	62	4.58	2.97	2	Cross	64	50
8	2.34	1.01	0.72	59	4.24	2.29	2	Cross	64	50

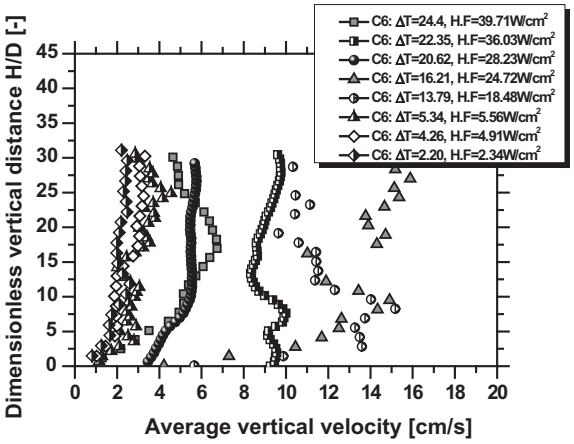

Fig. 9. Average vertical velocity versus dimensionless vertical distance for ethanol on the surface C6 (S = 800 μm). $\Delta T = T_w - T_{sat}$ and H.F is the imposed heat flux.

Similarly to what was observed with the previous surfaces, the velocity increases for $H/D = 0$ up to $10 < H/D < 20$. Then, the trend of the characteristic velocity is quite dependent on the imposed heat fluxes, as shown in Fig. 9.

Hence, for this surface, the characteristic velocity is observed to stabilize around a constant value, for the lowest and for the highest imposed heat fluxes. Instead, for intermediate values of the heat fluxes, one may observe larger characteristic velocities, which are however affected by stronger oscillations. These oscillations are no longer random and seem to be stabilized for higher heat fluxes, when the interaction mechanisms are stronger. It is argued that with the stronger interaction mechanisms, much more intense boiling process promotes mixing but also allows the formation of defined bubble columns in which subsequently detached bubbles are dragged, thus promoting a convective motion. Hence, one may argue that besides being an optimal distance between cavities, which will balance the positive effect of the larger number of cavities with a stronger horizontal coalescence, there is also an optimum distance which will actually stabilize the boiling process, which will contribute to the induced bulk convection. In this case, the process is already stable at the lowest and highest imposed heat fluxes (the result for the lowest heat flux is obviously due to a negligible interaction effect, but the highest may be already attributed to the aforementioned stabilizing effect).

To confirm this trend, one will further decrease S to 400 μm, for which the most relevant parameters are summarized in Table 6. Now the stabilizing effect of the interaction is very clear with this surface, as shown in Fig. 10: the velocity for increasing values of H/D is well defined for all the heat fluxes, thus after the initial increase of the characteristic velocity for $H/D > 0$, which is related to the detachment of the bubbles, there is an extended range of $7.5 < H/D < 15$ for which the characteristic velocity remains constant, with no significant oscillations. The high heat transfer rates promoted by this surface (which were already identified in Fig. 6) promote very fast evaporation so the braking effect which occurs as the bubbles reach the top of the pool is now more evident, as the velocity starts to decrease at lower values of H/D.

There is not a substantial variation on the velocity of the bubbles and actually, the absolute vertical velocity is slightly smaller for the surface with the "optimal S". However, the fact that the micro-patterns allow to establish a stable column of bubbles will definitely contribute to a stable bulk convection flow. This is obvious when comparing this surface with C7 (S = 1200 μm), for which the inadequate distance between cavities actually destabilizes the bubble motion leading to an inefficient heat transfer process. Such trend is clearer by relating the thermal characteristics with the bubble velocity, as discussed in the following sub-paragraph.

3.3. Relation between the micro-patterns, the bubble velocity and the heat transfer mechanisms

Fig. 11 relates the bubble characteristic velocity $V_{H/D=10-20}$ with the wall superheat for the four surfaces studied. The velocity increases with wall superheat and therefore with the imposed heat flux for all the surfaces. This is evident since the higher superheat will promote larger temperature differences between the surface and the liquid, which in turn will lead to larger density differences

Table 6
Complete panoramic of all the characteristics and main PIV parameters for surface C4 (S = 400 μm). t_{bp} is the time between pulses and I.A is the interrogation area.

No.	Heat flux [W/cm^2]	Heat transfer coefficient [W/cm^2 K]	Bubble departure diameter D [mm]	Bubble departure frequency f_d [Hz]	$f \cdot D$ [cm/s]	Characteristic velocity $V_{H/D=10-20}$ [cm/s]	t_{bp} [ms]	Corr. type	I.A [Px]	Overlap %
1	42.37	1.7	1.02	50.33	5.17	6.07	2	Cross	64	50
2	35.06	1.83	1.02	31.30	3.19	5.32	2	Cross	64	50
3	29.54	1.91	1.03	37.50	3..88	5.27	2	Cross	64	50
4	39.343	1.76	1.02	38.46	3.95	4.94	1	Cross	64	50
5	30.93	1.89	0.92	36.75	3.38	4.67	1	Cross	64	50
6	28.1	1.93	0.92	42.89	3.94	3.97	1	Cross	64	50
7	33.04	1.86	1.03	32.59	3.36	3.63	2	Cross	64	50
8	17.04	2.07	0.75	81.16	6.08	2.73	1	Cross	64	50

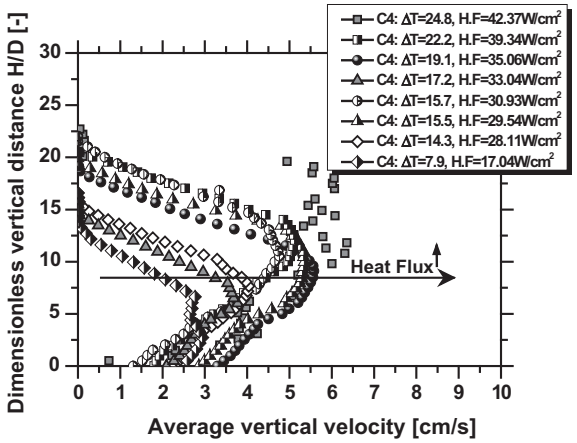

Fig. 10. Average vertical velocity versus dimensionless vertical distance for ethanol on the surface C4 (S = 400 μm). $\Delta T = T_w - T_{sat}$ and H.F is the imposed heat flux.

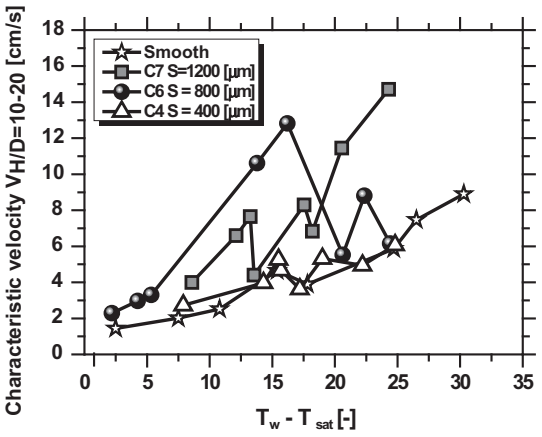

Fig. 11. Characteristic velocity versus wall superheated for the surfaces studied during the work.

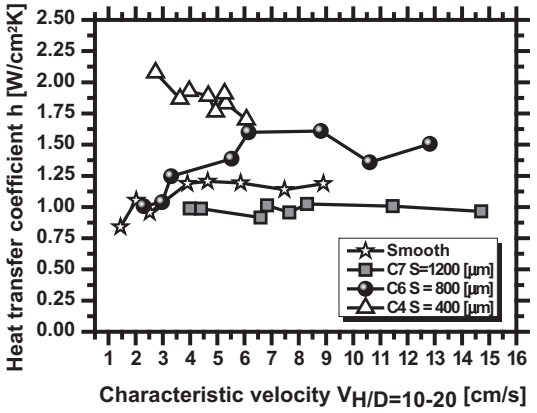

Fig. 12. Heat transfer coefficient versus characteristic velocity for the surfaces studied in this work.

between the liquid near and far from the wall, thus promoting natural convection.

Looking now at Fig. 12, which depicts the variation of the heat transfer coefficient with the characteristic velocity, the evaluation of the heat transfer coefficient is not straightforward since h is a complex function of many parameters related to bubble dynamics, flow motion and interaction mechanisms, which affects the three parcels identified by Han and Griffith [1].

Overall one may argue that the convection induced by bubble motion is quite reduced, in the present study. Actually, h decreases with the characteristic velocity for the best performing surface. Hence, the positive effect of increasing nucleation sites (under controlled coalescence) reached by the optimum distance S considerably improves the latent heat parcel, which is dominant mechanism, contrarily to the cases studied by Han and Griffith [1]. Such relative importance of the heat transfer parcels is consistent with the results since the surface promoting the largest characteristic velocities (C7, S = 1200 μm) gave rise to the lowest heat transfer coefficient, given the lowest number of active nucleation sites. The opposite trend is observed for the best performing surface C4, S = 400 μm. The best performance of this micro-patterned surface is also aided by the fact that this is the pattern which promotes better stability of the vertical bubbles motion, which is positive in removing the vapor away from the surface. On the other hand, the surface inducing the destabilization of the bubbles velocity (C7, S = 1200 μm) is again the one leading to the lowest heat transfer coefficient.

The analysis proposed here is not yet exhaustive, but suggests that the optimization of the surface topography for pool boiling heat transfer enhancement can be achieved by combining bubble dynamics, flow dynamics and heat transfer analysis. Image analysis combined with PIV is proposed as a good approach to perform this task efficiently.

4. Final remarks

The present work focuses on the hydrodynamic and heat transfer processes of pool boiling over surfaces patterned with micro-cavities, in the context of cooling applications. The results show that to assure an effective improvement of the heat transfer, the design of the micro-patterns must balance the positive effect of the micro-patterns in promoting the activation of the nucleation sites with the negative effect of an excessive interaction between them. Particular emphasis is given to the horizontal coalescence of the departed bubbles close to the wall, which is observed to cause the deterioration of the heat transfer coefficient, due to the formation of large vapor bubbles that isolate the surface from the liquid. The optimization of the surface patterns was achieved by varying the distance between the micro-cavities, S.

Characterizing the flow induced by the bubble motion is vital, since it allows understanding the relative importance of the three parcels of the heat transfer, namely, the natural convection, the latent heat and the bulk convection induced by bubble motion, as well as the consequent effect of the surface micro-patterning in each of them. In this context, an innovative analysis of the boiling process from micro-patterned surfaces is proposed here, which combines image post-processing with PIV measurements. Evaluation of the characteristic bubbles velocity obtained by PIV measurements evidences that the optimal pattern which balances the positive effect of increasing the parcel of liquid evaporation and the negative effect of the horizontal coalescence (with a distance between cavities S = 400 μm) also allows a more stable vertical bubble velocity, thus removing the vapor from the surface. However, the velocity of the bubbles for these surfaces is quite low, when compared to that of surfaces with a smaller number of cavities, i.e. with larger S. Hence, the convection induced by bubble motion is reduced in these optimal patterned surfaces, although the heat transfer coefficient is the highest. In line with this one may argue that the positive effect of increasing nucleation sites (under controlled coalescence) considerably improves the latent heat parcel, which is dominant. This may be so, since the surface

pattern promoting the largest velocities (C7, S = 1200 μm) has the lowest heat transfer coefficient, given the lowest number of active nucleation sites. Additionally, destabilization of the bubbles velocity is induced in this surface, which actually contributes to the deterioration of the heat transfer coefficient.

Acknowledgments

The authors are grateful to Fundação para a Ciência e a Tecnologia (FCT) for partially financing the research under the framework of Project PTDC/EME-MFE/109933/2009 and for supporting E. Teodori with a research Grant. A.S. Moita also acknowledges the contribution of FCT by supporting her with a Fellowship (Ref.: SFRH/BPD/63788/2009).

References

[1] C.Y. Han, P. Griffith, The mechanism of heat transfer in nucleate boiling, Technical Report No. 7673-19, Dep. Mech. Eng., M.I.T., 1962.
[2] C. Corty, A.S. Foust, Surface variables in nucleate boiling, Chem. Eng. Prog. Symp. Ser. 51 (17) (1955) 1–12.
[3] V. Chekanov, Interaction of centers during nucleate boiling, Teplofizika Vysokikh Temp. 15 (1977) 121–128.
[4] M. Sultan, R. Judd, Interaction of the nucleation phenomena at adjacent sites in nucleate boiling, J. Heat Transfer 105 (1983) 3–9.
[5] L. Zhang, M. Shoji, Nucleation sites interaction in pool boiling on the artificial surface, Int. J. Heat Mass Transfer 46 (3) (2003) 513–522.
[6] J.P. McHale, S.V. Garimella, Bubble nucleation characteristics in pool boiling of wetting liquid on smooth and rough surfaces, Int. J. Multiphase Flow 36 (2010) 249–260.
[7] A.S. Moita, E. Teodori, A.L.N. Moreira, Influence of surface topography and wettabiblity in the boiling mechanisms, in: 24th Annual Conference on Liquid Atomization and Spray Systems – ILASS2011, Estoril, Portugal, 2011.
[8] D.N. Nimkar, S.H. Bhavnani, R.C. Jaeger, Effect of nucleation sites spacing on the pool boiling characteristics of a structured surface, Int. J. Heat Mass Transfer 49 (2006) 2829–2839. To appear in J. Phys.: Conf. Ser. (JPCS).
[9] T. Sasaki, N. Nagai, Y. Murai, F. Yamamoto, Particle image velocimetry measurement of bubbly flow induced by alkaline water electrolysis, in: Proc. of PSFVIP-4, Chamonix, France, 2003.
[10] W. Cheng, Y. Murai, T. Sasaki, F. Yamamoto, Bubble velocity measurement with a recursive cross correlation PIV technique, Flow Meas. Instrum. 16 (2005) 35–46.
[11] A.S. Moita, E. Teodori, A.L.N. Moreira, Enhancement of pool boiling heat transfer by surface micro-structuring, J. Phys.: Conf. Ser. 395: 012175 (2012) http://dx.doi.or/10.1088/1742-6596/395/1/012175.
[12] E. Teodori, A.S. Moita, A.L.N. Moreira, Effects of surface micro-structuring on the nucleation mechanisms, in: IV National Conference on Fluid Mechanics, Thermodynamics and Energy MEFTE 2012, 2012.
[13] H.T. Phan, N. Caney, P. Marty, S. Colasson, J. Gavillet, How does wettability influence nucleate boiling?, CR. Mec. 337 (2009) 251–259.
[14] A.S. Moita, A.L.N. Moreira, Scaling the effects of surface topography in the secondary atomization resulting from droplet/wall interactions, Exp. Fluids 52 (3) (2012).
[15] S.E. Mohamed, H. Bostanci, Thermal Challenges in Next Generation Electronic Systems, in: Joshi, Garimella (Eds.), Millpress, Rotterdam, 2002. ISBN 90-77017-03-8.
[16] S. Chaptun, M. Watanabe, M. Shoji, Nucleation site interaction in pool nucleate boiling on a heated surface with triple artificila cavities, Int. J. Heat Mass Transfer 47 (2004) 3583–3587.
[17] M. Raffel, C. Willert, S. Wereley, J. Kompenhans, Particle Image Velocimetry: A Practical Guide, second ed., Springer Verlag, Heidelberg, 2007.